Stationnary Convection Diffusion between two Co-Axial Cylinders.

Franck Plouraboué, Charles Pierre

Stationary convection-diffusion between two co-axial cylinders

F. Plouraboué, * C. Pierre [a]

[a] *Département de Mathématiques et Statistique,*
Université d'Ottawa 585 King Edward KIN 6N5,
Ottawa, Ontario, Canada.

Abstract

In this note, we examine the high Péclet number limit of the stationary extended Graetz problem for which two families of real and imaginary eigenvalues are associated respectively with a downstream convective relaxation and the upstream diffusive establishment. The asymptotic behavior of both families of eigenvalues is studied, in the limit of large Péclet number and thin wall, which bring to the fore a single parameter dependence, previously mentioned in the literature from numerical investigations [2]. The fully developed region is specifically studied thanks to the first eigenvalue dependence on the Péclet number, on the thermal conductivity coefficients and on the diameter ratio of the cylinders. The effective transport between the fluid and the solid is investigated through the evaluation of the fully developed Nusselt number and compared with available experimental measurements.

Key words: micro-systems, heat transfer, spectral analysis, asymptotic

Nomenclature:

D^I,D^{II}	Thermal diffusivity in the fluid (I) and in the solid (II)
F_R	Eigenfunction in the solid cylinder
G	Graetz eigenfunction
I	Dimensionless asymptotic parameter
J_0, J_1	Zeroth and first Bessel functions of the first kind
k^I, k^{II}	Thermal conductivity coefficents
Y_0, Y_1	Zeroth and first Bessel functions of the second kind
Nu	Nusselt number
S	Surface of the cylinder
r_a, r_b	Internal radius of the inner and outer cylinder
Pe	Péclet number
r	Radial coordinate

* Corresponding author, Address: Institut de Mécanique des Fluides de Toulouse

UMR CNRS-INPT/UPS No.5502 Avenue du Professeur Camille Soula

31400 Toulouse France, tel 33 5 61 28 58 80, fax 33 5 61 28 58 78

Email address: plourab@imft.fr (F. Plouraboué,).

$R = \frac{r_b}{r_a}$:	Aspect ratio between the inner and the outer cylinder
P	Fluid pressure
S	Surface of the inner pipe
T	Temperature
T_0	Reference temperature at infinity
$\Theta = T - T_0$	Intrinsic temperature
U	Averaged longitudinal velocity
u	Fluid longitudinal velocity
z	Longitudinal coordinate
Greek symbols	
$\eta = \frac{r}{r_a}$	Dimensionless radial coordinate
λ	Eigenvalue of the coupled thermic problem
$\Phi(a, b, z)$	Confluent hyper-geometric function
$\zeta = \frac{z}{r_a}$	Dimensionless longitudinal coordinate

1 Introduction

We hereby analyze some special limit of the Extended Graetz problem using variable separation eigenfunctions. The mathematical and numerical solutions

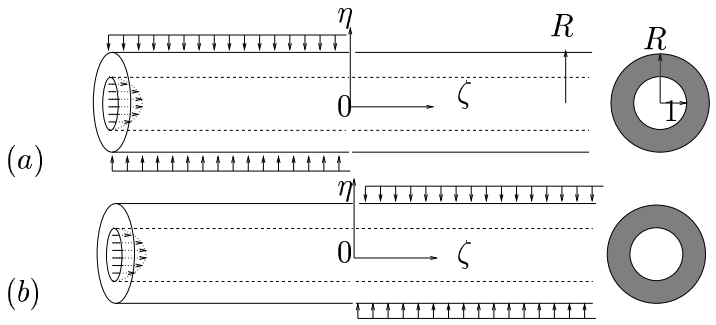

Fig. 1. Schematic representation of the two symmetrical configurations under study.

for this problem has been developed obtained in numerous previous contribution [5, 6, 11, 10, 9]. From the precursory contribution of Papoutsakis *et al* [5, 6], a complete representation of the solution relies on an orthogonal eigenfunction expansion of this problem, independently from the applied boundary conditions for the external cylinder, the input and the output conditions. The core of any explicit numerical computation of the temperature field relies on the evaluation of a subset of the infinite discrete spectrum of eigenvalues, and eigenfunctions.

In this note we focus on some simple expression for the asymptotic behavior of the solution, which put forward a simple parameter already heuristically proposed in previous contribution. The effective transfer between the tube and the co-axial solid cylinder in the fully developed region is studied through the computation of the Nusselt number in section four. A comparison with the available experimental results is discussed in the last section.

2 General solution and eigenvalue problem

The extended Graetz problem is considered for two complementary configurations sketched on figure 1 that we will subsequently refer to as 1a and 1b. The

following non-dimensional variables are introduced to describe the problem,

$$\eta = \frac{r}{r_a}, \quad \zeta = \frac{z}{r_a}, \quad R = \frac{r_b}{r_a}, \qquad Pe = \frac{2Ur_a}{D^I},$$

where r_b is the radius of the solid co-axial cylinder. A fully developed hydrodynamic flow inside the tube is considered. The velocity longitudinal component u along the z axis of the tube has a Poiseuille parabolic profile which is proportional to the mean applied pressure gradient $\partial_z P$:

$$u = \frac{1}{4}\partial_z P(r_a^2 - r^2) = \frac{2U}{r_a^2}\left(r_a^2 - r^2\right), \qquad U = \frac{1}{S}\int_S u dS = \frac{2}{r_a^2}\int_0^{r_a} ur\, dr,$$

where U is the averaged fluid velocity inside the tube having section S and radius r_a. Only axi-symmetric boundary conditions will be considered in the following. The non-dimensional Stationary convection-diffusion of heat is described by

$$\begin{aligned} Pe\partial_\zeta \Theta &= \tfrac{1}{\eta(1-\eta^2)}\partial_\eta\left(\eta\partial_\eta\Theta\right) \text{ in } \quad I, \\ \Delta\Theta &= 0 \quad \text{in} \quad II, \end{aligned} \tag{1}$$

where $\Theta = T - T_0$ is a relative temperature built on the reference temperature T_0 in the fluid tube I and the solid region II at $z \to +\infty$ for configuration 1a and at $z \to -\infty$ for configuration 1b, as already used in [5, 6]. We restrict our attention to the solution region where there is an adiabatic isolated solid cylinder *i.e* $\zeta > 0$ in configuration 1a, and $\zeta < 0$ in configuration 1b.,

$$\partial_\eta \Theta^{II}(R, \zeta) = 0 \tag{2}$$

Firstly we are looking at far-field decreasing boundary conditions,

$$\Theta^I \to \Theta^{II} \to 0 \qquad |\zeta| \to \infty \tag{3}$$

While the temperature and flux equilibrium between the fluid and solid region reads

$$k^I \partial_\eta \Theta^I(1,\zeta) = k^{II} \partial_\eta \Theta^{II}(1,\zeta) \tag{4}$$

$$\Theta^I(1,\zeta) = \Theta^{II}(1,\zeta) \tag{5}$$

Where k^I, k^{II} are the thermal conductivity in the fluid and in the solid. One can find a general solution to the problem (1) by writing it as :

$$\begin{aligned} \Theta^I(\eta,\zeta) &= \Sigma_n \theta_{n\pm} G(\lambda_{\pm n},\eta)\ e^{-\lambda_{\pm n}^2 \zeta/Pe} \\ \Theta^{II}(\eta,\zeta) &= \Sigma_n \theta_{n\pm} F_R(\tfrac{\lambda_{\pm n}^2}{Pe}\eta)\ e^{-\lambda_{\pm n}^2 \zeta/Pe}, \end{aligned} \tag{6}$$

where

$$F_R\left(\frac{\lambda_n^2}{Pe}\eta\right) = J_0\left(\frac{\lambda_n^2}{Pe}\eta\right) Y_1\left(\lambda_n^2 \frac{R}{Pe}\right) - J_1\left(\lambda_n^2 \frac{R}{Pe}\right) Y_0\left(\frac{\lambda_n^2}{Pe}\eta\right)$$

is the linear combinations of the Bessel harmonic eigenfunctions [1] which fulfills the radial adiabatic boundary condition (2). $G(\lambda,\eta)$ is the Graetz function:

$$G(\lambda,\eta) = e^{-\lambda\eta^2/2}\Phi(\frac{1}{2} - \frac{\lambda}{4}, 1, \lambda\eta^2),$$

where $\Phi(a,b,z)$ is the confluent hyper-geometric function [1] (sometimes referred to as ${}_1F_1$) which possesses two a and b parameters and one variable z. Unlike the solution of the Graetz problem, the solutions families (6) explicitly depend on the Péclet number, on the radius ratio of the fluid and solid region and on the conductivity ratio k^I/k^{II} through condition (4).

One of the most interesting features of these solutions is that in the region where no flux is applied, one finds a longitudinal exponential decrease in temperature whose characteristic length is directly related to the first eigenvalue of

the problem. The forward eigenvalue λ_{+n} is associated with the temperature relaxation convected downstream in 1a configuration while the "backward" eigenvalue λ_{-n} is associated with the upstream temperature rise induced by the solid conduction in Figure 1b configuration. Using the solution family (6), imposing the interface coupling conditions (4) and (5) leads to the following eigenvalue problem on λ_n:

$$\frac{k^I Pe}{k^{II}} \frac{F_R(\lambda_n^2/Pe)}{F_R'(\lambda_n^2/Pe)} = \lambda_n \frac{\Phi(\frac{1}{2} - \frac{\lambda_n}{4}, 1, \lambda_n)}{2\Phi'(\frac{1}{2} - \frac{\lambda_n}{4}, 1, \lambda_n) - \Phi(\frac{1}{2} - \frac{\lambda_n}{4}, 1, \lambda_n)} , \tag{7}$$

where $'$ denotes the derivative of functions with respect to their variables.

3 Large Péclet number and small diameter limit

In the following sections the fully developed region where the first eigenfunction is dominant will be our main focus. The region for which the first eigenfunction prevails over all the other ones is given by the ζ values for which $(\lambda_2^2 - \lambda_1^2)\zeta/Pe > 3$. The amplitude of this fully developed mode is the projection of the concentration field at $\zeta = 0$ with the first eigenfunction. We will not be interested by this amplitude in the following, focusing on the first eigenvalue and Nusselt number. We investigate the large Péclet number limit which is equivalent with a thin solid region. In this limit $Pe \gg 1$ the ratio $F_R'(\lambda_n^2/Pe)/F_R(\lambda_n^2/Pe) \simeq \lambda_n^2(1-R)R/Pe$. Thus, one has merely to solve the simplified eigenproblem:

$$-\Phi(\frac{1}{2} - \frac{\lambda_n}{4}, 1, \lambda_n) + 2\Phi'(\frac{1}{2} - \frac{\lambda_n}{4}, 1, \lambda_n) = \frac{k^{II}}{k^I} \frac{R(R-1)}{Pe^2} \lambda_n^3 \Phi(\frac{1}{2} - \frac{\lambda_n}{4}, 1, \lambda_n), \tag{8}$$

to find the eigenvalue λ_n. Direct numerical results of the coupled problem (1) have been carried out by [2] in this limit and have shown that the typical entry

length in figure (1b) configuration depends on a single parameter I

$$I = \frac{k^{II}}{k^I}\frac{R(R-1)}{2Pe^2}, \tag{9}$$

only. Eigenvalue problem (8) shows precisely the same dependence on the geometrical, physical and hydrodynamical parameters of the problem.

3.1 Forward eigenvalue λ_{+n}

Forward eigenvalues are associated with the downstream decrease of temperature in figure (1a) configuration. In the limit of infinite Péclet number, eigenvalues λ_{+n} have finite values defined by the following transcendental equations

$$\Phi(\frac{1}{2} - \frac{\lambda^{\infty}_{+n}}{4}, 1, \lambda^{\infty}_{+n}) = 2\Phi^{'}(\frac{1}{2} - \frac{\lambda^{\infty}_{+n}}{4}, 1, \lambda^{\infty}_{+n}), \tag{10}$$

In this limit λ_{+n} does not depend on the three parameters of the problem R, Pe and k^I/k^{II} and exactly coincides with the Neumann-Graetz problem eigenvalues. For large but finite Péclet numbers and for a small aspect ratio, one can linearize (8) to get the asymptotic behavior of the eigenvalues, which only depends on I

$$\lambda_{+n} - \lambda^{\infty}_{+n} = \frac{2{\lambda^{\infty}_{+n}}^3\alpha_n}{\pi}\frac{k^{II}R(1-R)}{k^I \mathrm{Pe}^2} \tag{11}$$

where $\alpha_n = 1/\left((\frac{1}{2} - \frac{\lambda^{\infty}_{+n}}{4})(\frac{3}{2} - \frac{\lambda^{\infty}_{+n}}{4})\Phi(\frac{5}{2} - \frac{\lambda^{\infty}_{+n}}{4}, 3, \lambda^{\infty}_{+n}) - (1/4)\Phi(\frac{1}{2} - \frac{\lambda^{\infty}_{+n}}{4}, 1, \lambda^{\infty}_{+n})\right)$. When the diffusivity ratio decreases to zero, or when the solid radius cylinder decreases to 1, the transport in region I and II becomes decoupled and, of course, one finds the asymptotic Graetz-Neumann solution. Again, the asymptotic validity of the linearization (11) is interesting to compare with numerical computations. The full eigenproblem (7) has been solved with a Newton

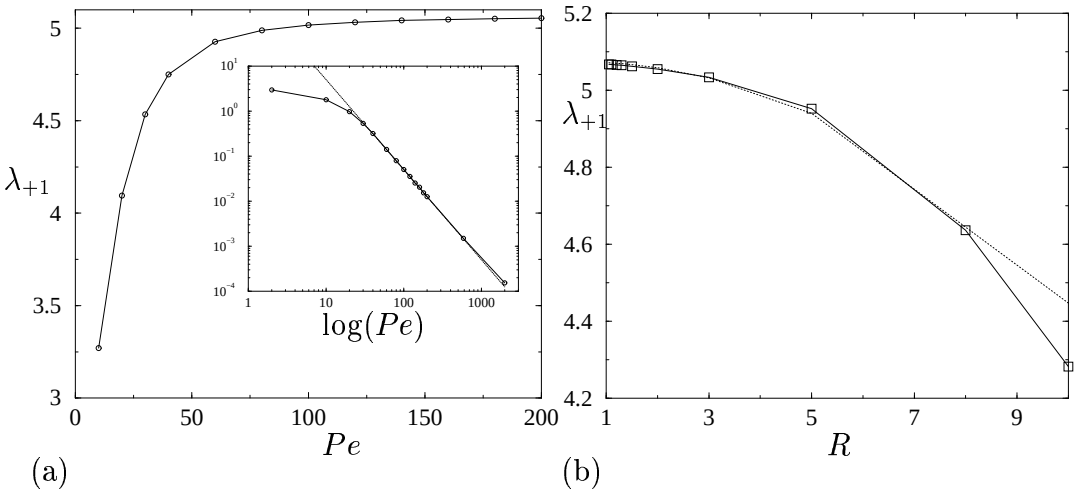

Fig. 2. (a) First eigenvalues λ_{+1} versus Pe, for $R = 2$, $\frac{k^I}{k^{II}} = 1$. The inset represents a log-log representation of the difference $\lambda_{+1} - \lambda_{+1}^{\infty}$ with $\lambda_{+1}^{\infty} = 5.067505$ versus the Péclet number; the asymptotic (11) is represented with dotted lines. (b) Same conventions as in figure (a) versus the aspect ratio R for $Pe = 200$. Dotted line illustrates the asymptotic (11)

method using the numerical evaluation of the confluent hyper-geometric function proposed in [4]. The eigenvalues have been tracked with a continuation method. Figures 2(a) and (b) display the behavior of the first eigenvalue λ_{+1}. We used a Figure 2(a) shows that when the diameter of the outer cylinder is twice as large as that of the inner one and when diffusivity is the same in both, linearization (11) gives good approximation for the first eigenvalue even for moderate values of the Péclet Number. A careful inspection of the numerical values represented in Figure 2(a) shows that the prediction (11) is already 4% accurate for Péclet number value as low as 30. Figure 2(b) compares the proposed scalings for the eigenvalues as a function of the cylinder aspect ratio R. It shows that even if the asymptotic prediction is supposed to hold for $1 - R \ll 1$, it is still very good for large values of R when the Péclet number is large.

Backward eigenvalues are associated with the upstream decrease of temperature in figure (1b) configuration. The eigenvalue λ_{-1} has previously been studied with direct numerical simulations by [2] when the outer cylinder is thin ($R-1 \ll 1$). They have described the temperature decrease observed in the domain $\zeta < 0$ of Figure 1b configuration. Using these numerical simulations as a heuristic base, [7] found the simplified eigenproblem (8) by averaging the temperature field in the solid. In this domain, fluid convection in region I and solid diffusion in region II play antagonist roles for the temperature rises from the far field applied reference to the $\zeta = 0$ heat source. The more convection there is, the smaller the temperature of establishment length will be, while conversely, the more diffusion in the solid, the larger the distance for the temperature to be established. Thus establishing length tends to zero as the Péclet number goes to infinity while conversely the eigenvalue λ_{-1} tends to infinity. The divergence of this backward eigenvalue with the Péclet number is illustrated on figure 3a.

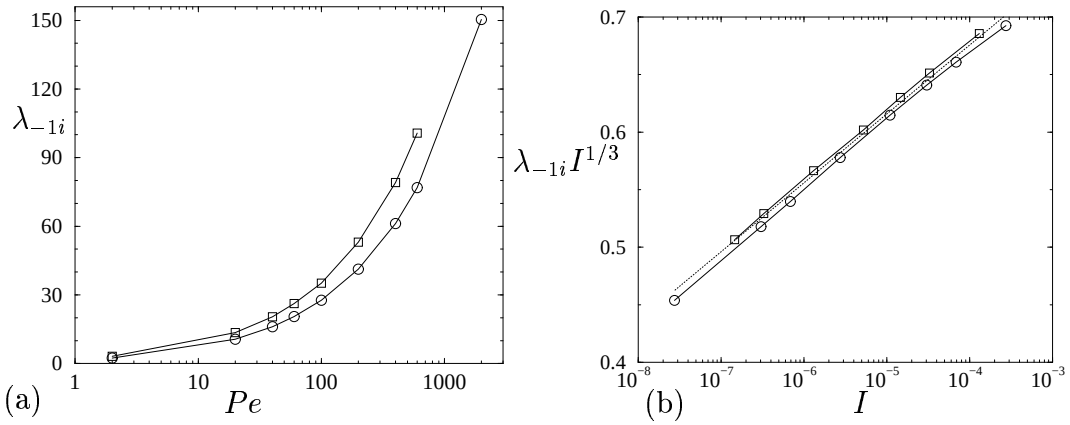

Fig. 3. (a) Imaginary part of the first backward eigenvalue λ_{-1} versus Pe, for $R = 1.1$ with circle symbols and $R = 1.05$ for square symbols with $\frac{k^I}{k^{II}} = 1$. (b) Same conventions for $\lambda_{-1i}I^{1/3}$ versus parameter I in semi-logarithmic representation.

The full eigenvalue problem (7) is solved here and represented on Figure 3a. In section 5 it is compared to the numerical solution of the approximated problem (8) and to experimental measurements. On the other hand, the approximated eigenproblem (8) can be used to find an asymptotic expression for the eigenvalue λ_{-n} with the Péclet number

$$\frac{\Phi'(1/2-\lambda_{-n}/4,1,\lambda_{-n})}{\Phi(1/2-\lambda_{-n}/4,1,\lambda_{-n})} = \frac{1}{2} + \frac{k^{II}R(R-1)}{k^I 2}(\frac{\lambda_{-n}^3}{Pe^2}) \tag{12}$$

Nevertheless it is not easy to get the asymptotic behavior of the confluent hyper-geometric function when both its first parameter and its variable tend to infinity. [3] have thoroughly discussed the numerous asymptotic behavior of function $\Phi(a,b,\lambda)$ in this limit, for fixed values of the ratio $a/4\lambda$. In the presently interesting limit where $4a/\lambda \to 1$, their results show that the logarithmic derivative of the confluent geometric function does not diverge algebraically when $a \to \infty$ and $\lambda \to \infty$. The numerical calculation confirms this result leading to logarithmic dependence on λ_{-1}. As illustrated on figure 3b the asymptotic behavior of the first upstream eigenvalue λ_{-1} display a logarithmic dependence with the single parameter I, which collapse into a single master curve when changing the aspect ratio parameter R. This leads to the following expression of the backward eigenvalue dependence on the Péclet number,

$$\lambda_{-1} = I^{-1/3}\,(0.026\ln I + 0.915) \tag{13}$$

The linear behavior with the logarithm of parameter I requires two constants that have been obtained from fitting the numerical computation sketched on Figure 3b.

4 Fully developed transfer

The Nusselt number is defined by the non dimensional flux between region I and II:

$$\mathrm{Nu}(\zeta) = \frac{1}{\Theta_\mathrm{b}(\zeta) - \Theta_\mathrm{w}(\zeta)} \frac{\partial \Theta}{\partial \mathrm{n}}, \tag{14}$$

where $\Theta_w = \Theta(1,\zeta)$ is the wall temperature and Θ_b is given by

$$\Theta_b = \frac{1}{S^I U} \int_{S^I} u \Theta^I dS^I, \qquad\qquad U = \frac{1}{S^I} \int_{S^I} u dS^I,$$

where S^I is the region I disk surface, and Θ_b is the flow weighted averaged temperature or "mixing cup" temperature. Another definition is sometimes found in the literature omitting the $\Theta_w(\zeta)$ term of the denominator. We have kept this definition here to be able to compare with some experimental data in the backward configuration. Looking for a simplified far field expression for the Nusselt number one finds that its fully developed asymptotic behavior reaches a constant value which depends only on the first eigenfunction and eigenvalue. This can be done from averaging with a "mixing cup" weight the convection-diffusion equation (1) in the liquid. This leads to a relation between Θ_b and the transverse temperature variation at the inner wall:

$$\frac{1}{4} Pe \partial_\zeta \Theta_b = \partial_\eta \Theta(1,\zeta) \tag{15}$$

Using this relation and solution (6), one can then find the fully developed approximation of these fields in the limit where $|\zeta| \gg 1$,

$$\Theta_w \simeq \quad \theta_1 \quad e^{-\lambda_1/2}\, e^{-\lambda_1^2 \zeta/Pe} \quad \Phi(\frac{1}{2} - \frac{\lambda_1}{4}, 1, \lambda_1) \tag{16}$$

$$\Theta_b \simeq -4 \frac{\theta_1}{\lambda_1}\, e^{-\lambda_1/2}\, e^{-\lambda_1^2 \zeta/Pe} \left(2\Phi'(\frac{1}{2} - \frac{\lambda_1}{4}, 1, \lambda_1) - \Phi(\frac{1}{2} - \frac{\lambda_1}{4}, 1, \lambda_1) \right). \tag{17}$$

From these expressions, one is then able to find an explicit formulation of the fully-developed Nusselt number from using definition (14) :

$$\mathrm{Nu} = \frac{\lambda_1}{\frac{\Phi(\frac{1}{2}-\frac{\lambda_1}{4},1,\lambda_1)}{-2\Phi(\frac{1}{2}-\frac{\lambda_1}{4},1,\lambda_1)+4\Phi'(\frac{1}{2}-\frac{\lambda_1}{4},1,\lambda_1)} + \frac{2}{\lambda_1}}. \tag{18}$$

Although explicit, this expression can be even further simplified in the context of the large Péclet numbers and small solid diameter previously considered in Eq.(8) for which it simply reads

$$\mathrm{Nu} \simeq 4\lambda_1^4 I, \tag{19}$$

where, again, the limit $I = \frac{k^{II}}{k^I}\frac{R(R-1)}{2Pe^2} \ll 1$ is considered. Now, using the asymptotic expression obtained in (11) leads to the explicit formula, in terms of the physical, geometrical, and hydrodynamical parameters of the problem, for the forward eigenvalue :

$$\mathrm{Nu}_+ = 2\lambda_{+1}^{\infty\,4}\left(1 - 8\frac{\lambda_{+1}^{\infty\,3}\alpha_1}{\pi}\frac{\mathrm{k^{II}}}{\mathrm{k^I}}\frac{\mathrm{R(R-1)}}{\mathrm{Pe^2}}\right)\frac{\mathrm{k^{II}}}{\mathrm{k^I}}\frac{\mathrm{R(R-1)}}{\mathrm{Pe^2}}. \tag{20}$$

It is interesting to note that, to the leading order neglecting $O(1/Pe^2)$ effects, the forward transfer is not increasing with the Péclet number. On the contrary it decreases quadratically with this parameter. This result is not intuitive since increasing the flow enhances the temperature longitudinal gradient. The typical axial decreasing length of the temperature field ℓ_+ scales as $\ell_+ \sim Pe/\lambda_{+1}^2$. When the fluid is increased this length asymptotically increases linearly with the Péclet number. A side effect of this increase is nevertheless that, conversely, normal gradients shrink when the stationary temperature field is stretched by convection, so that the transverse gradient scales as $1/\ell_+$. Most of the temperature variations are concentrated at the tube center, and

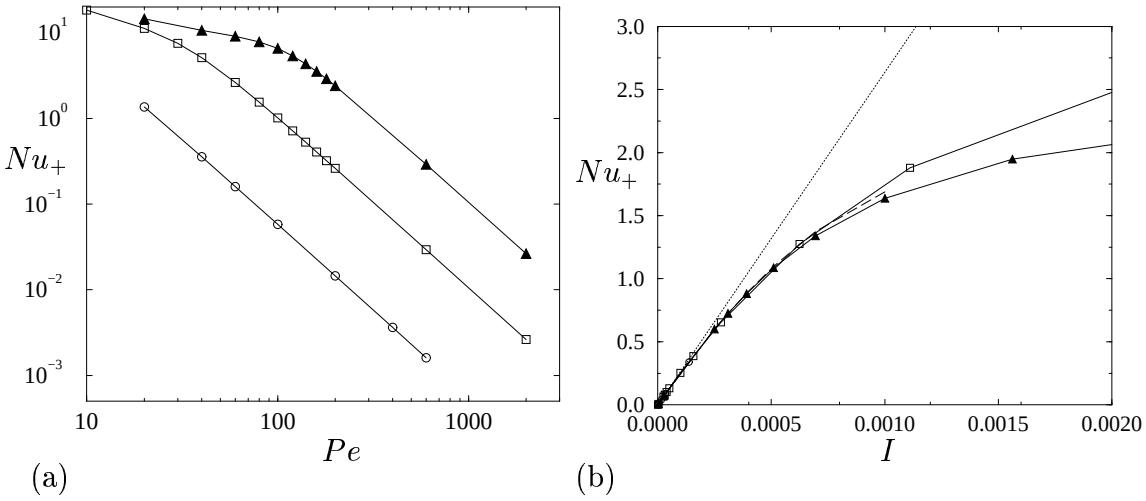

Fig. 4. Fully developed Forward Nusselt number for different parameters. Bullet symbols are associated with $R = 1.1$, square symbols for $R = 2$ and black triangular symbols with $R = 5$. (a) Versus the Péclet number. (b) Versus the parameter I defined in (9). The leading order asymptotic behavior (20) is shown with dotted lines, while the next order is represented with long dashed lines.

decrease rapidly to reach a quasi-constant value near the tube inner wall. In this limit, the temperature difference between the liquid and the wall is thus grossly proportional to ℓ_+. Moreover, since the radial temperature gradient scales as $1/\ell_+$, the Nusselt number which is the product between the inverse of temperature difference and the temperature gradient should then scale as $Nu_+ \sim 1/\ell_+^2$, so that $Nu_+ \sim 1/Pe^2$. These physical arguments thus allows to recover the leading order scaling (20). Both asymptotic are compared with the numerical solution of (19) in figure 4. One can observed the convergence to the quadratic leading order dependence with the Péclet number found in (20) on figure 4a for different values of the aspect ratio R. This figure again shows that the range of value of R for which the the asymptotic regime applies can be quite broad reaching values as large as 5, for moderate value of the Péclet number of the order of 100. Figure 4b compares the leading and first order

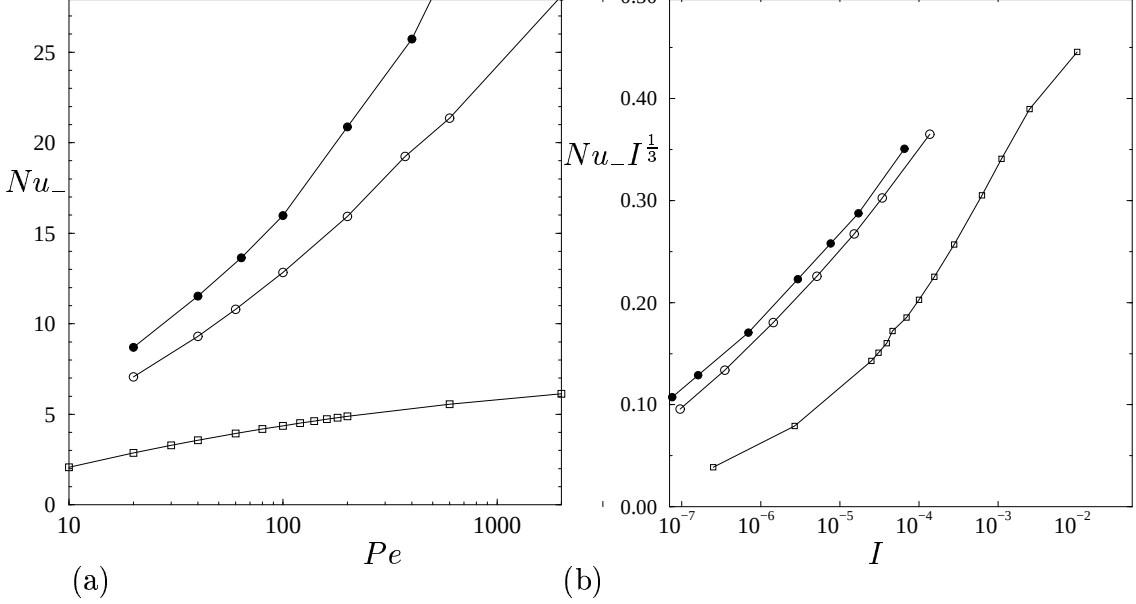

Fig. 5. Fully developed Backward Nusselt number for different parameters. Black Bullet symbols are associated with $R = 1.05$, while white ones are for $R = 1.1$ and square symbols for $R = 2$. (a) Versus the Péclet number. (b) Versus the parameter I defined in (9).

asymptotic behaviors given above, while all different sets collapse into a single master curve when plotted as a function of parameter I, in the limit of small values of this parameter.

In the case of the backward Nusselt number, an asymptotic expression can also be obtained from (13) and (19), in the limit of small values of parameter I, so that one finds :

$$\mathrm{Nu}_- = \mathrm{I}^{-1/3} 4 \left(0.026 \ln \mathrm{I} + 0.915\right)^4 . \tag{21}$$

This asymptotic behavior leads to larger and larger Nusselt numbers when increasing the Péclet number, as opposed to the forward case. This trend is confirmed from the computation of the Nusselt number from (19) depicted on figure 5a, from which it can be observed that the Nusselt number reaches

values an order of magnitude larger than in the forward case, even for moderate values of the Péclet number. The transfer from the solid to the fluid is thus much more important in the backward direction, even if the length-scale ℓ_- associated with the typical axial decreasing length of the temperature field is much more smaller. From the definition of parameter I given in (9), it is easy to see that the leading order scaling in Péclet, is $\mathrm{Nu}_- \sim \mathrm{Pe}^{2/3}$ up to logarithmic corrections. This leading order behavior can be grossly understood from the same physical argument previously developed for the forward Nusselt number, indicating that in the backward case it should scale as $\mathrm{Nu}_- \sim 1/\ell_-^2$. Since $\ell_- \sim Pe/\lambda_{-1}^2 \sim Pe^{-1/3}$, we then find that the transfer should scale as $\mathrm{Nu}_- \sim \mathrm{Pe}^{2/3}$. The logarithmic correction that have been previously obtained should be viewed as a particularity of the cylindrical geometry that has been chosen here, and should not appear in the similar planar problem. It is also interesting to note that the validity range of the asymptotic behavior (21) is much more restrain than in the forward case as illustrated on figure 5b. For moderate values of the Péclet number such as 100, the value of R for which it applies are not larger than 1.1. One can observed for instance that the behavior of the Nusselt number associated with $R = 2$ on figure 5b does not collapse on the same master curve associated with the asymptotic limit. In the limit of extremely small values of parameter I it should nevertheless merge with the other curves.

5 Comparison with experiments

It is interesting to compare theory and experiments using the single parameter I to collapse different geometrical, physical or hydrodynamical situations

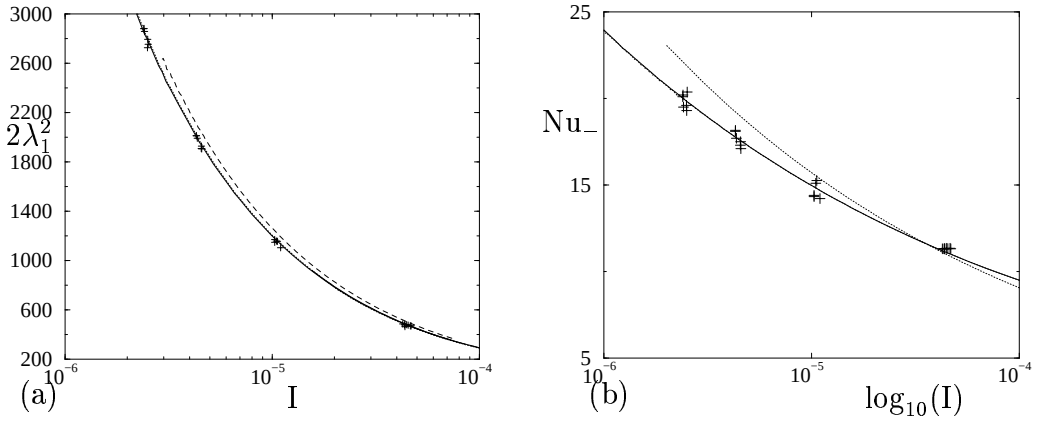

Fig. 6. (a) $2\lambda_1^2 \equiv m$, parameter used in [8]) plotted versus the non-dimensional parameter I. The numerical solution of (7) is represented with continuous line for $1 - R = 10^{-2}$ and dashed lines for $1 - R = 10^{-1}$. Numerical solution of the approximated eigenvalue problem (8) represented with dotted lines. The experimental results of [8]) are represented with crosses.(b) Same conventions as Figure (a) for the comparison between theory and experiments for the Nusselt number

when the solid cylinder wall is small. To our knowledge, only experimental measurements in the figure 1b configuration are available in the literature. Using a copper tube the radius of which is one tenth of the inner cylinder, and using water as a working fluid [8]) carried out a large number of experiments for Péclet numbers ranging from 1180 to 5000. The heat conductivity of copper being much larger than that of water, the conductivity ratio was in their case equal to $k^{II}/k^I = 549 \pm 19$. Two major parameters are interesting to compare with the experimental measurements. First, let us consider the longitudinal entry length ℓ_- (called m in [8]) characterizing the exponential decrease in temperature. This parameter is determined from the log-linear best slope fit of the temperature variations measured with thermocouples placed along the longitudinal direction of the external face of the solid cylinder. The 25 data measurements of [8] are represented on figure 6a and compared with theoretical predictions. A prediction in the case of the thin solid wall limit is derived

from solving equation (8). It is interesting to note that this prediction is in very good agreement with experimental measures, as already found in [7]. This approximated theory compares very closely to the exact solution of Eq.(7) in the case of radius ratio $R = 10^{-2}$. A difference between this approximated theory and the exact one is nevertheless observed in the case of $R = 10^{-1}$ which corresponds to experimental conditions. Thus, even if the theoretical predictions are very satisfyingly close to experiments, a discrepancy of about 10% is observed, which could be within the experimental error bars. Another interesting parameter to compare with the experiments is the Nusselt number represented on figure 6b. The Nusselt number can not be directly measured in the experiments; it is rather extrapolated from temperature measurements. Here again, theory and experiments can compare in a satisfactory way, within a 10% difference.

Conclusion

We found simple asymptotic expression for the first upward and backward eigenvalues of the extended Graetz-problem. Those results should be useful for testing numerical estimation or experimental results in the limit of large Péclet number.

Acknowledgments

We thanks M. Quintard and A. Bergeon for stimulating discussions.

References

[1] M. Abramowitz and I. Stegun. *Handbook of mathematical functions.* Dover publication, inc., new-york, 1972.

[2] M. A. Cotton and J. D. Jackson. *Numerical methods in thermal problems*, volume IV, pages 504–515. R. W. Lewis and K. Morgan eds, Pineridge Press, Swansea, 1985.

[3] A. Erdélyi and C. A. Swanson. Asymptotics forms of wittakers confluent hypergeometric functions. *Memoirs of the American Mathematical society*, 25:929, 1957.

[4] M. Nardin, W. F. Perger, and A. Bhalla. Algorithm 707 conhyp : a numerical evaluator of the confluent hypergeometric function for complex arguments of large magnitudes. *ACM transactions on mathematical software*, 18(3):345–349, 1992.

[5] E. Papoutsakis, D. Ramkrishna, and H. C. Lim. The extended graetz problem with diriclet wall boundary conditions. *Appl. Sci. Res.*, 36:13–34, 1980.

[6] E. Papoutsakis, D. Ramkrishna, and H. C. Lim. The extended graetz problem with prescribed wall flux. *AIChE J.*, 26:779–787, 1980.

[7] S. Piva. Axial wall conduction preheating effects in high péclet number laminar forced convection. *Int. J. Heat Mass Transfer*, 39(16):3511 – 3517, 1996.

[8] S. Piva and G Pagliarini. Estimation of unknown parameters from exponential heating of laminar flow. *Expl. Thermal Fluid Sci.*, 8:21 – 27, 1994.

[9] A. Silva Telles, E. M. Queiroz, and G. Elmôr Filho. Solutions of the extended graetz problem. *Int. J. Heat Mass Transfer*, 44(2):471–483,

2001.

[10] B. Weigand, M. Kanzamar, and H. Beer. The extended graetz problem with piecewise constant wall heat flux for pipe and channel flows. *International Journal of Heat and Mass Transfer*, 44(20):3941–3952, 2001.

[11] B. Weigand and D. Lauffer. The extended graetz problem with piecewise constant wall temperature for pipe and channel flows. *International Journal of Heat and Mass Transfer*, 47(24):5303–5312, 2004.